Impact of Environmental Scattering on Transmit Nulling Performance

Peter Vouras
Naval Research Laboratory, Radar Division
4555 Overlook Avenue S.W., Washington D.C., 20375, USA

Abstract—**Promising techniques have recently been developed for creating nulls in the transmit sidelobes of a radar by using the signal from a nearby auxiliary antenna. In operational settings, the performance of these nulling techniques will be sensitive to electromagnetic scattering from objects in the vicinity of the antennas. This paper presents a theoretical analysis of the impact of environmental and multipath scattering on transmit nulling performance for a radar system comprised of a main antenna and an auxiliary. A case study example is described for scattering off the ocean surface.**

I. Introduction

It is possible to create a spatial null in the transmit sidelobes of a radar antenna by radiating a signal from an auxiliary antenna that is equal in amplitude but 180 degrees out of phase with the signal from the main antenna in the desired null direction. The two signals will subtract in the far field to form a null. The efficacy of this approach will depend on the presence of electromagnetic scattering from the environment and nearby objects. The theoretical analysis presented in this paper analyzes the impact of environmental scattering on transmit nulling performance. The framework for this analysis follows the approach described in [1] for sidelobe cancellers.

Figure 1 illustrates a general scattering geometry. The radar main antenna, either a reflector or a phased array, and the auxiliary antenna are modelled as a linear array with two elements. The spacing between the elements is denoted by d. The transmit signal $s(t)$, radiating through the sidelobes of the main antenna at an angle θ_d arrives at the desired null location via a direct path and is taken as a unity gain, zero delay reference. Another version of $s(t)$ reflects off a multipath scatterer with reflection coefficient ρ_m at an angle θ_r and arrives at the null location via an indirect path with delay τ_m. The signal radiated from the auxiliary antenna follows a direct path to the null location with unity gain and delay τ_d relative to the direct path main signal. Also, a scattered version of the auxiliary signal arrives at the null location with reflection coefficient ρ_a and delay τ_a. The propagation delays associated with the direct and reflected paths can be computed as

$$\tau_d = \left(\frac{d}{c}\right)\sin\theta_d \,, \tag{1}$$

$$\tau_r = \left(\frac{d}{c}\right)\sin\theta_r \,, \tag{2}$$

$$\tau_a = \tau_m + \tau_r \,, \tag{3}$$

where c is the speed of light.

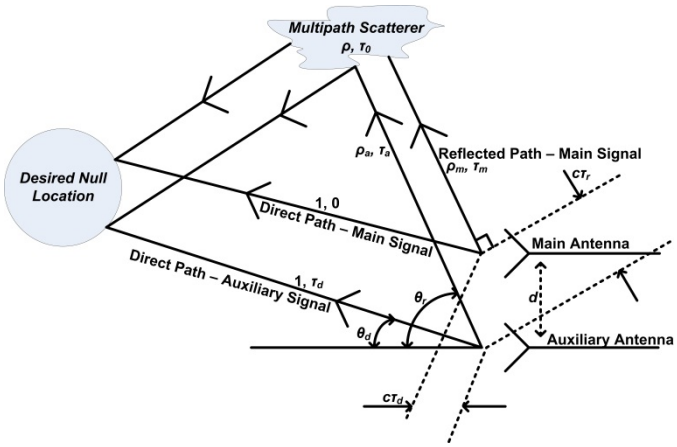

Fig. 1. Environmental Scattering Geometry

Ideally, the direct and scattered signals from the main antenna are all correlated replicas of each other that arrive at the null location with different delays. Therefore, they can be cancelled by incorporating a tapped delay line (TDL) in the auxiliary channel with J taps spaced T_s seconds apart (Fig. 2). The minimum sampling rate associated with the tap delay spacing should be the Nyquist rate, or twice the highest frequency radiated by the auxiliary antenna.

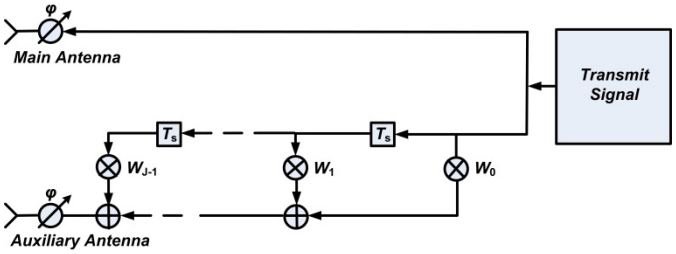

Fig. 2. Auxiliary Antenna with Tapped Delay Line

If the transmit signal is $s(t)$, the real signal arriving at the null location from the main antenna is

$$m(t) = s(t) + \rho_m s(t - \tau_m). \tag{4}$$

The noise radiated through the main antenna will be ignored since it is uncorrelated with the noise from the auxiliary

antenna. The total signal at the null location arriving from the auxiliary antenna is

$$a(t) = s(t-\tau_d) + \rho_a s(t-\tau_m-\tau_r) + n_a(t), \quad (5)$$

where $n_a(t)$ is the noise transmitted through the auxiliary antenna. The expressions for the autocorrelation and cross-correlation functions of $s(t)$, $n_a(t)$, $m(t)$, and $a(t)$ are

$$R_s(\tau) = E\left[s(t+\tau)s^*(t)\right] = \gamma\,\mathrm{sinc}(B\tau), \quad (6)$$

$$R_n(\tau) = E\left[n_a(t+\tau)n_a{}^*(t)\right] = \mathrm{sinc}(B\tau), \quad (7)$$

$$R_m(\tau) = E\left[m(t+\tau)m^*(t)\right] = \left(1+|\rho_m|^2\right)R_s(\tau) + \rho_m R_s(\tau-\tau_m) + \rho_m^* R_s(\tau+\tau_m),$$

$$R_a(\tau) = E\left[a(t+\tau)a^*(t)\right] = \left(1+|\rho_a|^2\right)R_s(\tau) + \rho_a R_s(\tau-\tau_m+\tau_d-\tau_r) + \rho_a^* R_s(\tau+\tau_m-\tau_d+\tau_r) + R_n(\tau), \quad (9)$$

$$R_{ma}(\tau) = E\left[m(t+\tau)a^*(t)\right] = R_s(\tau+\tau_d) + \rho_a^* R_s(\tau_m+\tau_r+\tau) + \rho_m R_s(\tau+\tau_d-\tau_m) + \rho_m\rho_a^* R_s(\tau_r+\tau). \quad (10)$$

In the above equations, the symbol * denotes complex conjugation, B represents the signal bandwidth, and γ is the signal-to-noise ratio.

II. Minimum Mean Square Error Solution

If the auxiliary channel has J taps spaced T_s seconds apart, then a spatial null in the antenna transmit pattern can be created when the tap weights w_i are chosen to minimize the Mean Squared Error (MSE) criterion

$$\xi = E\left[|r(t)|^2\right] \quad (11)$$

where $r(t)$ is defined as the residual error signal

$$r(t) = m(t) - \sum_{i=0}^{J-1} w_i a(t-iT_s). \quad (12)$$

The total delay introduced in the auxiliary channel with this architecture is $(J-1)T_s$. In a closed-loop transmit nulling system using a feedback sensor, adaptation will continue until the residue is uncorrelated with each delayed auxiliary signal, i.e.

$$E\left[r(t)a^*(t-iT_s)\right] = 0, \qquad i = 0,1,\ldots,J-1. \quad (13)$$

The optimal solution which minimizes the residue power is the Wiener solution,

$$\mathbf{w}_{opt} = \mathbf{R}^{-1}\mathbf{r} \quad (14)$$

where $\mathbf{R}$ is the $J\times J$ auxiliary signal covariance matrix

$$[\mathbf{R}]_{ij} = E\left[a(t-jT_s)a^*(t-iT_s)\right] = R_a[(i-j)T_s] \quad (15)$$

and $\mathbf{r}$ is the $J\times 1$ cross-correlation vector with elements

$$\mathbf{r}_i = E\left[m(t)a^*(t-iT_s)\right] = R_{ma}(iT_s). \quad (16)$$

For a single tap weight, (14) becomes a scalar equation.

The residue power attained with the optimal auxiliary tap weights $\mathbf{w}_{opt}$ is the lowest possible [2],

$$P = P_{\min} = P_m - \mathbf{r}^{\mathbf{H}}\mathbf{R}^{-1}\mathbf{r}, \quad (17)$$

where $P_m = R_m(0)$ is the power of the direct and multipath signals radiated from the main antenna. If the tap weights $\mathbf{w}$ are not optimal, then the residue power is

$$P = P_m - \mathbf{w}^{\mathbf{H}}\mathbf{r} - \mathbf{r}^{\mathbf{H}}\mathbf{w} + \mathbf{w}^{\mathbf{H}}\mathbf{R}\mathbf{w}. \quad (18)$$

The null depth d, defined relative to the total ambient signal power at the null location originating from the main antenna, is

$$d = \frac{P}{P_m}. \quad (19)$$

This quantity is analogous to the cancellation ratio of a sidelobe canceller.

III. Least Squares Solution

The signals $m(t)$ and $a(t)$ can be written as the convolution of $s(t)$ with the impulse responses of the main and auxiliary transmission channels, $h_m(t)$ and $h_a(t)$ respectively [1]. In other words,

$$m(t) = s(t) * h_m(t), \quad (20)$$

$$a(t) = s(t) * h_a(t) + n_a(t), \quad (21)$$

where the main and auxiliary channel impulse responses are

$$h_m(t) = \delta(t) + \rho_m\delta(t-\tau_m), \quad (22)$$

$$h_a(t) = \delta(t-\tau_d) + \rho_a\delta(t-\tau_m-\tau_r). \quad (23)$$

The channel frequency responses, $H_m(\omega)$ and $H_a(\omega)$, defined by

$$H_m(\omega) = 1 + \rho_m e^{-j\omega\tau_m}, \quad (24)$$

$$H_a(\omega) = e^{-j\omega\tau_d} + \rho_a e^{-j\omega(\tau_m+\tau_r)}, \quad (25)$$

are the Fourier transforms of $h_m(t)$ and $h_a(t)$.

An ideal filter at the input to the auxiliary antenna would first apply the inverse filter $H_a^{-1}(\omega)$ to remove the effect of multipath in the auxiliary transmission path and then would apply the filter $H_m(\omega)$ to introduce the multipath associated with $m(t)$. Thus the frequency response of the ideal composite filter applied to the auxiliary signal is

$$H(\omega) = H_a^{-1}(\omega) H_m(\omega). \quad (26)$$

The impulse response $h(t)$ of $H(\omega)$ will have infinite duration. A practical closed-loop transmit nulling system will adaptively approximate the infinite impulse response of $h(t)$ with a FIR filter $g(t)$ that has J taps,

$$g(t) = \sum_{k=0}^{J-1} g[k]\delta(t - kT_s). \quad (27)$$

Thus the estimation problem reduces to matching the FIR impulse response $g(t)$ to the IIR impulse response $h(t)$ as closely as possible. The optimal FIR filter in the mean square error sense will be a truncated version of the infinite impulse response [1]. The signal residue remaining at the null location can be approximated by

$$r(t) = m(t) - g(t) * a(t) = [h(t) - g(t)] * a(t). \quad (28)$$

The residue power is equal to

$$P_r = E\left[|r(t)|^2\right] = \frac{1}{2\pi}\int_{-\infty}^{\infty} |H_e(\omega)|^2 S_a(\omega) d\omega \quad (29)$$

where

$$H_e(\omega) = H(\omega) - G(\omega) \quad (30)$$

and the power spectral density corresponding to $R_a(\tau)$ is

$$\begin{aligned} S_a(\omega) = {} & \left(1 + |\rho_a|^2\right) S_s(\omega) + \rho_a S_s(\omega) e^{-j\omega(\tau_m - \tau_d + \tau_r)} \\ & + \rho_a^* S_s(\omega) e^{j\omega(\tau_m - \tau_d + \tau_r)} + S_n(\omega), \end{aligned} \quad (31)$$

with

$$S_s(\omega) = \gamma \,\mathrm{rect}\left(\frac{\omega}{2\pi B}\right) \quad (32)$$

and $S_n(\omega)$ equal to the noise power spectral density.

The integral in (29) can be evaluated by sampling $H_e(\omega)$ and $S_a(\omega)$ in the frequency domain. To estimate $G(\omega)$ in (30) it is necessary to truncate samples of the infinite impulse response $h(t)$. In turn, the impulse response $h(t)$ can be estimated from an inverse Fourier transform of samples of $H(\omega)$. However, care must be taken to avoid aliasing in the time domain when calculating the inverse Fourier transform of frequency samples of $H(\omega)$. Suppose it is assumed that the effective duration of $h(t)$ is T seconds. Then the frequency samples of $H(\omega)$ should be spaced $1/T$ Hertz apart. Furthermore, if the desired spacing between the filter taps $g[k]$ is T_s seconds, then the frequency samples of $H(\omega)$ should extend up to a frequency of $1/T_s$ Hertz. In summary, the frequency response $H(\omega)$ should be sampled at the frequencies

$$\omega[k] = \frac{2\pi k}{T}, \quad 0 \le k \le \frac{T}{T_s}. \quad (33)$$

IV. Simulated Results

Figure 3 plots the transmit null depth as defined in (19) versus the normalized delay of the scattered main antenna signal for seven values of the real reflection coefficient ρ_m, with the reflection coefficient ρ_a set equal to zero. A normalized delay equal to unity implies no overlap between the direct path and the scattered signals; whereas a normalized delay of zero corresponds to complete overlap. Other parameter values include B = 31250 Hz, θ_d = 10°, θ_r = 40°, d = 10λ, and γ = 100. The auxiliary channel filter had one tap weight set equal to the Wiener solution given by (14). In this case, the tap weight was computed with perfect knowledge of the direct and reflected signals. This plot shows that for values of the reflection coefficient ρ_m less than 0.1 and for normalized multipath delays less than 0.1; the attainable null depths are at least 35 dB below the ambient signal level. The plot also shows that as the relative delay increases between the direct and reflected main antenna signals at the null location, and thereby their overlap decreases, the null depth decreases because the duration of the auxiliary signal is not long enough to cancel both the direct and indirect main signals. For example, if there is no overlap between the direct and indirect main signals at the null location and ρ_m = 1, then the null depth is equal to -3 dB.

Figure 4 illustrates the case where ρ_a is set equal to 0.2 and the reflection coefficient ρ_m is allowed to vary. The plot shows that when ρ_m becomes equal to ρ_a the main and the auxiliary transmission channels are perfectly matched and the transmitted signals cancel completely to create the maximum null depth.

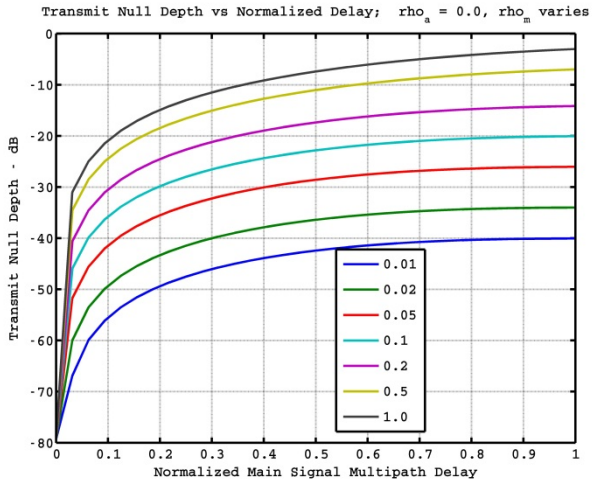

Fig. 3. Transmit Null Depth vs Signal Delay ($\rho_a = 0$)

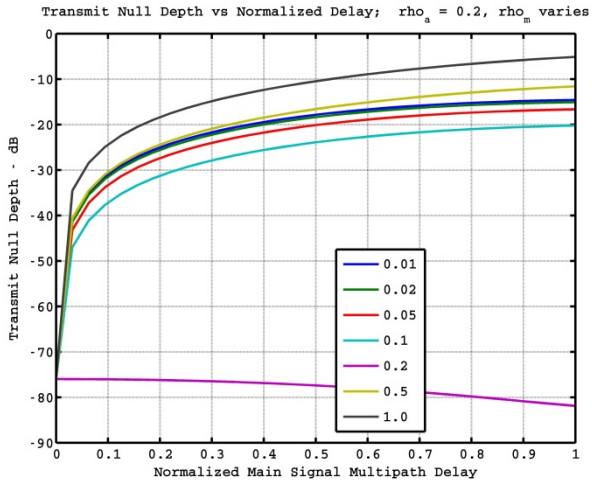

Fig. 4. Transmit Null Depth vs Signal Delay ($\rho_a = 0.2$)

Figure 5 illustrates the case where the auxiliary tap coefficient is incorrect while $\rho_a = 0$ and ρ_m is allowed to vary. In this scenario, the covariance matrix used to compute the Wiener solution does not include the scattered main signal. As the plot suggests, the scattered main signal is not cancelled at the null location, and it therefore contributes to the residue power and raises the null depth. For example, if $\rho_a = 0$ and $\rho_m = 0.5$ with no overlap (i.e. normalized delay equals 1) between the direct and indirect main signals, then the residue power equals $0.5^2/(1^2+0.5^2)$ or -7 dB. If $\rho_a = 0$ and $\rho_m = 0.5$ with total overlap (i.e. normalized delay equals 0) between the direct and indirect main signals, then the residue power equals $0.5^2/1.5^2$ or -9.5 dB.

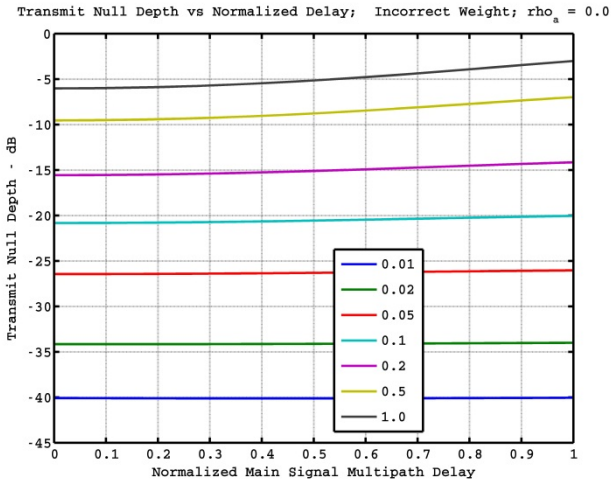

Fig. 5. Transmit Null Depth vs Signal Delay (Incorrect Tap Weight)

The performance of the tapped delay line architecture is illustrated in Fig. 6. Here the null depth is plotted as a function of the number of taps J in the TDL for different values of the sampling frequency corresponding to the tap spacing. The sampling frequency varies in multiples of the signal bandwidth (from 2 to 8 times). The effective duration of the impulse response $h(t)$ is assumed to be 0.1 msec. The total delay T_{aux} introduced in the auxiliary channel due to the FIR filter $g[k]$ is equal to $(J\text{-}1)T_s$. The parameters $\tau_m = 4$ μsec and $B = 2$ MHz.

A striking feature of the plots in Fig. 6 is the step-like decrease in null depth as the number of taps increases. Considering only the case where the sampling frequency is 2 times the signal bandwidth, Fig. 7 reveals that the step reductions in null depth occur at multiples of T_{aux} to the indirect path delay τ_m.

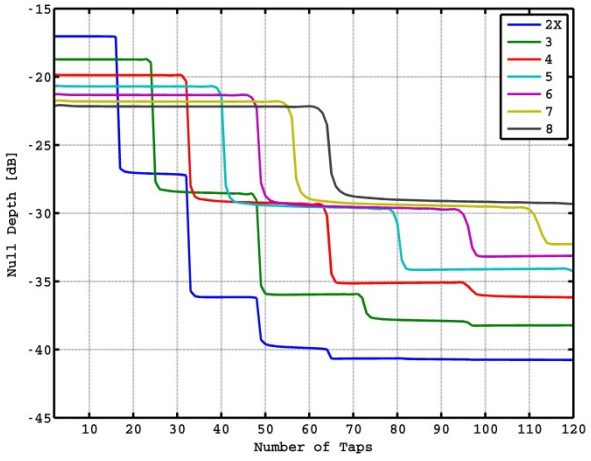

Fig. 6. Null Depth vs Number of Taps

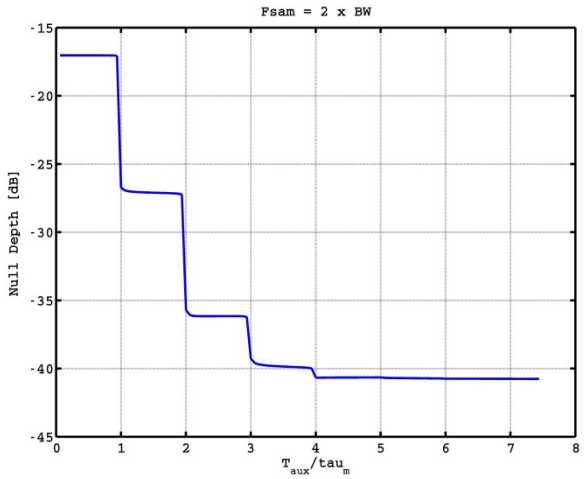

Fig. 7. Null Depth vs T_{aux}/τ_m

V. Ocean Surface Scattering

This section considers the most likely multipath scenario for naval radars − scattering off the ocean surface. Figure 8 illustrates the relevant multipath geometry. An antenna with elevation angle θ_e transmits sidelobe energy toward the desired null location. The radiated signal follows a direct path R_d to the null location and an indirect path corresponding to $R_1 + R_2$. Accordingly, the direct and multipath signals will have a relative phase difference at the null location due to the different path lengths travelled. The phase difference corresponding to a path length difference Δ is $2\pi\Delta/\lambda$ radians. There will also be a phase change φ that occurs during reflection off the ocean's surface and a phase difference between the signals due to the antenna pattern factor at different pointing directions, which is ignored here for simplicity. Thus the total phase difference α between the multipath signal and the direct path signal is

$$\alpha = \frac{2\pi\Delta}{\lambda} + \varphi \ , \tag{34}$$

and the complex exponential representation of the reflection coefficient at the reflection point is

$$\Gamma = \rho_0 e^{-j\alpha} \ . \tag{35}$$

Here, the real scalar ρ_0 represents the ratio of the intensity of the reflected wave to that of the incident wave. To analyze the effects of ocean scattering on transmit nulling performance fully using the framework developed in Section II, it is necessary to determine Γ.

Referring to Fig. 8, the angle ψ at the reflection point of the incident ray is referred to as the grazing angle. The values of ρ_0 and α are both functions of the grazing angle. By using extensive algebraic manipulations and trigonometry described in [4], it is possible to solve for ψ for different values of the elevation angle θ_e, the slant range to the null location R_d, and the height of the radar antenna above the Earth's surface h_1. For example, Fig. 9 illustrates the grazing angle as a function of slant range for eleven antenna elevation angles and an antenna height of 30 meters above the Earth's surface. For the same antenna configuration, the relative phase difference at L−band between the direct and reflected signals due to the different path lengths travelled is shown in Fig. 10. Computed values of φ are illustrated in Fig. 11 for each of the antenna elevation angles considered.

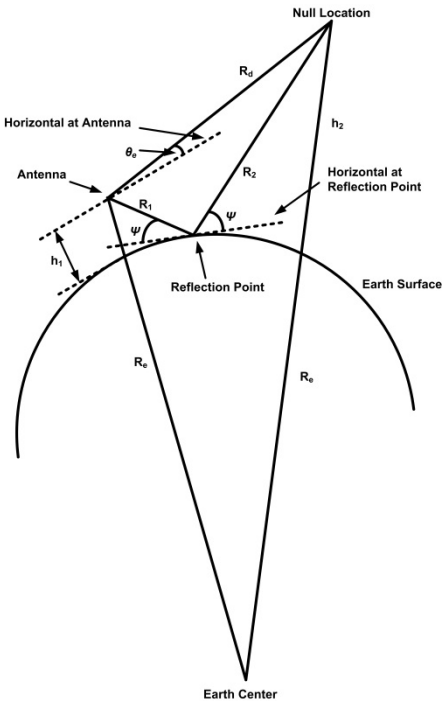

Fig. 8. Multipath Geometry for Ocean Scattering

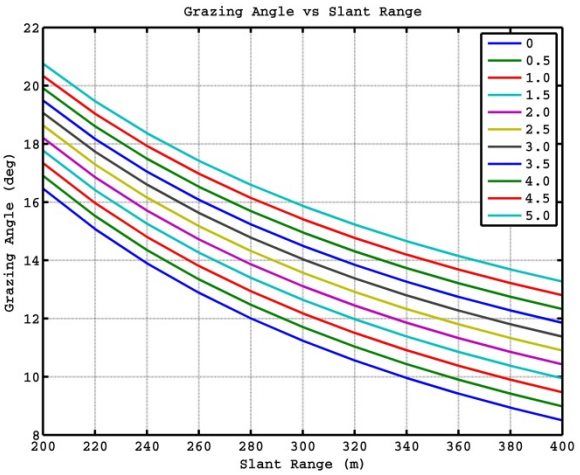

Fig. 9. Grazing Angle vs Slant Range (h_1 = 30 m)

An extensive body of work exists in the literature relevant to computing the reflection coefficient Γ from sea surface scattering [5-17]. The simplest case is for specular reflection

off a smooth sea. A mathematical expression for Γ derived in [4] for horizontally polarized radiation is

$$\Gamma = \frac{\sin\psi - \sqrt{\varepsilon_c - \cos^2\psi}}{\sin\psi + \sqrt{\varepsilon_c - \cos^2\psi}}. \quad (36)$$

The constant ε_c is referred to as the dielectric constant of seawater. For reflection from a smooth sea at low grazing angles with horizontal polarization of the radar waves, ρ_0 is almost identically one.

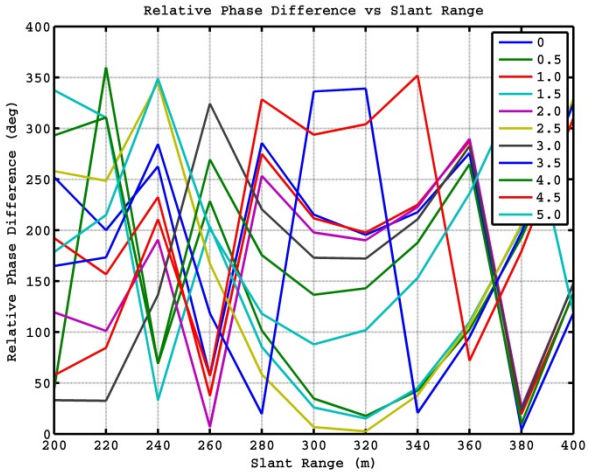

Fig. 10. Relative Phase Difference vs Slant Range (h_1 = 30 m)

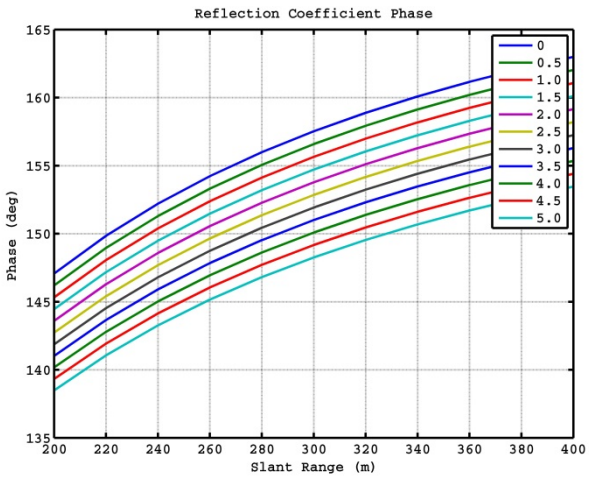

Fig. 11. Phase Shift Due to Reflection vs Slant Range (h_1 = 30 m)

VI. Conclusion

The theoretical analysis presented in this paper suggests that environmental scattering can have a significant impact on transmit nulling performance for a system architecture with a main antenna and an auxiliary. In particular, the detrimental effects of multipath scattering can be mitigated by increasing the number of tap weights in the auxiliary antenna channel.

References

1. D. R. Morgan and A. Aridgides, "Adaptive Sidelobe Cancellation of Wide-Band Multipath Interference," *IEEE Transactions on Antennas and Propagation*, Vol. 33, No. 8, pp. 908-917, August 1985.
2. S. Haykin, *Adaptive Filter Theory*, 3rd ed., Upper Saddle River, NJ: Prentice Hall, 1996.
3. B. Porat, *A Course in Digital Signal Processing*, New York, NY: John Wiley & Sons, 1997.
4. L. V. Blake, *Radar Range-Performance Analysis*, Silver Spring, MD: Munro Publishing, 1991.
5. M. I. Skolnik, *Radar Handbook*, 3rd ed., New York, NY: McGraw Hill, 2008.
6. M. W. Long, *Radar Reflectivity of Land and Sea*, 3rd ed., Boston, MA: Artech House, 2001.
7. J. Stapleton, J. Cavanagh, G. D. Dockery, R. McDonald, J. P. Reilly, J. Goldhirsh, M. Newkirk, R. Blase, J. Hoyle, and R. Galejs, "Natural Environmental Models for Shipboard Radars," Naval Surface Warfare Center Technical Report TR-99/151, Dahlgren, VA, September 2001.
8. C. I. Beard, "Remote Sensing of Ocean Significant Wave Height by Forward Scattering: Examples from L-Band Data," Naval Research Laboratory Memorandum Report MR-3968, Washington DC, April 18, 1979.
9. C. I. Beard, D. L. Drake, and C. M. Morrow, "Measurements of Microwave Forward Scattering from the Ocean at L-Band," *Proceedings NAECON Conference*, Dayton, OH, May 13-15, 1974.
10. F. E. Nathanson, J. P. Reilly, and M. N. Cohen, *Radar Design Principles: Signal Processing and the Environment*, 2nd ed., New York, NY: McGraw Hill, 1991.
11. H. D. Griffiths, W. A. Al-Ashwal, K. D. Ward, R. J. A. Tough, C. J. Baker, and K. Woodbridge, "Measurement and Modelling of Bistatic Radar Sea Clutter," *IET Radar, Sonar and Navigation*, Vol. 4, Iss. 2, pp. 280-292, 2010.
12. A. Khenchaf, "The Brewster Angle Effect on Sea Surface Scattering for Near-Grazing Incidence," *Proceedings IEEE International Geoscience and Remote Sensing Symposium*, Hamburg, Germany, 28 June - 2 July, 1999.
13. A. Khenchaf, "Sea Surface Scattering for Near-Grazing Incidence," *Proceedings Oceans '99*, Seattle, WA, September 13-16, 1999.
14. W. A. Al-Ashwal, A. Balleri, H. D. Griffiths, W. J. Micelli, K. Woodbridge, "Measurements of Bistatic Radar Sea Clutter," *Proceedings IEEE Radar Conference*, Kansas City, MO, May 23-27, 2011.
15. T. P. Kochanski, M. J. Vanderhill, J. V. Zolotarevsky, T. Fariss, "Low Illumination Angle Bistatic Sea Clutter Measurements at X-Band," *Proceedings Oceans '92*, Newport, RI, October 26-29, 1992.
16. K. D. Ward and P. W. Shepherd, "Bistatic Radar Sea Clutter Experiments and Spatial Coherence," *Proceedings International Conference Radar '92*, Brighton, England, October 12-13, 1992.
17. T. Oyedokun and M. Inggs, "Design and Evaluation of a Sea Clutter Simulator," *Proceedings IEEE International Geoscience and Remote Sensing Symposium*, Vancouver, Canada, July 24-29, 2011.